BIOCHEMISTRY
including biophysical chemistry & molecular biology

Article

pubs.acs.org/biochemistry

Distinctive Effects of Domain Deletions on the Manganese-Dependent DNA Polymerase and DNA Phosphorylase Activities of *Mycobacterium smegmatis* Polynucleotide Phosphorylase

Mihaela-Carmen Unciuleac and Stewart Shuman*

Molecular Biology Program, Sloan-Kettering Institute, New York, New York 10065, United States

Supporting Information

ABSTRACT: Polynucleotide phosphorylase (PNPase) plays synthetic and degradative roles in bacterial RNA metabolism; it is also suggested to participate in bacterial DNA transactions. Here we characterize and compare the RNA and DNA modifying activities of *Mycobacterium smegmatis* PNPase. The full-length (763-aa) *M. smegmatis* PNPase is a homotrimeric enzyme with Mg^{2+}•PO_4-dependent RNA 3′-phosphorylase and Mg^{2+}•ADP-dependent RNA polymerase activities. We find that the enzyme is also a Mn^{2+}•dADP-dependent DNA polymerase and a Mn^{2+}•PO_4-dependent DNA 3′-phosphorylase. The Mn^{2+}•DNA and Mg^{2+}•RNA end modifying activities of mycobacterial PNPase are coordinately ablated by mutating the putative manganese ligand Asp526, signifying that both metals likely bind to the same site on PNPase. Deletions of the C-terminal S1 and KH domains of mycobacterial PNPase exert opposite effects on the RNA and DNA modifying activities. Subtracting the S1 domain diminishes RNA phosphorylase and polymerase activity; simultaneous deletion of the S1 and KH domains further cripples the enzyme with respect to RNA substrates. By contrast, the S1 and KH domain deletions enhance the DNA polymerase and phosphorylase activity of mycobacterial PNPase. We observe two distinct modes of nucleic acid binding by mycobacterial PNPase: (i) metal-independent RNA-specific binding via the S1 domain, and (ii) metal-dependent binding to RNA or DNA that is optimal when the S1 domain is deleted. These findings add a new dimension to our understanding of PNPase specificity, whereby the C-terminal modules serve a dual purpose: (i) to help capture an RNA polynucleotide substrate for processive 3′ end additions or resections, and (ii) to provide a specificity filter that selects against a DNA polynucleotide substrate.

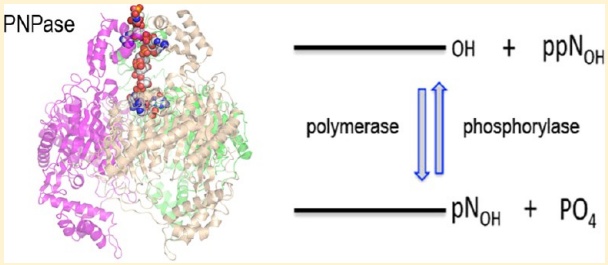

Polynucleotide phosphorylase (PNPase) is a versatile enzyme that plays synthetic and degradative roles in bacterial RNA metabolism.[1] In its degradative mode, PNPase catalyzes processive phosphorolysis of the 3′-terminal phosphodiesters of RNA chains to yield nucleoside diphosphate (NDP) products. It its polymerase mode, PNPase uses NDPs as substrates to add NMPs to the 3′-OH terminus of RNA chains while expelling inorganic phosphate (P_i). The polymerase reaction is the microscopic reversal of the phosphorolysis reaction, and both require a divalent cation. Insights to the structural organization and catalytic mechanism of PNPase have emerged from crystal structures of exemplary bacterial and eukaryal PNPases.[2−6] PNPases are ring-shaped homotrimers with a central channel that admits RNA and within which the active site is located. The channel accommodates single-stranded RNA but excludes duplex RNA. Each protomer is composed of five domain modules (Figure 1A). Two RNase PH-like domains comprise the core of the trimeric ring. The metal-binding site is located within the distal PH domain.[4] An α-helical module separating the PH domains is disposed on the inferior surface of the ring. The C-terminal KH and S1 domains are on the opposite face of the ring and are conformationally mobile. In the *Caulobacter* PNPase structure, the three KH modules of the trimer form a narrow aperture that contacts the RNA and through which the RNA chain is threaded en route to the central cavity.[6]

Several studies have addressed the contributions of the KH and S1 domains to the activity of PNPase by deleting these modules, singly or in combination.[3,5,7,8] In one report, deletion of the S1 domain of *Escherichia coli* PNPase reduced the RNA phosphorylase specific activity by a factor of 50 and elicited a similar decrement in RNA binding affinity.[8] In another study of the *E. coli* protein, deleting both the S1 and KH domains reduced RNA binding affinity by a factor of 8.[3] By contrast, deleting the S1 domain of human PNPase did not affect RNA binding affinity or RNA phosphorylase activity, although mutations in the KH domain exerted severe effects.[5] The disparate effects of C-terminal domain deletions on PNPase activity may reflect the use of different reaction conditions of varying stringency[8] and/or variable effects of the domain deletions on the stability or conformation of the trimeric PNPase ring.[3] Nonetheless, the emerging theme is that the KH and S1 domains are relevant for RNA binding at a distance from the active site.

Received: March 5, 2013
Revised: April 4, 2013
Published: April 5, 2013

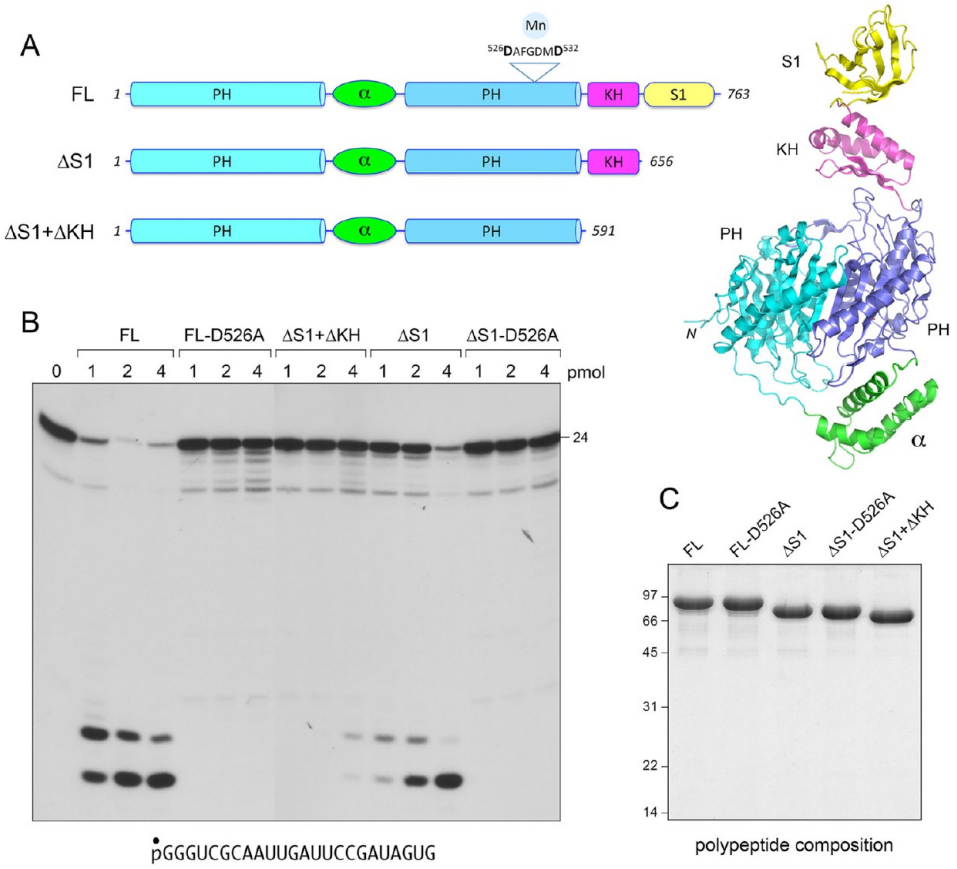

Figure 1. Domain organization, purification, and RNA phosphorylase activity of mycobacterial PNPase. (A) The modular domain structure of full-length (FL) *M. smegmatis* PNPase is shown. The putative Mn^{2+}-binding site in the distal PH domain is highlighted. Truncated versions Δ*S*1 and Δ*S*1+ΔKH are shown below the FL polypeptide. The tertiary structure of the homologous FL PNPase of *Caulobacter crescentus* (pdb ID 4AIM) is depicted at right. (B) Phosphorylase reaction mixtures (10 μL) containing 20 mM Tris-HCl (pH 7.5), 5 mM $MgCl_2$, 0.5 mM ammonium phosphate, 1 pmol (0.1 μM) of 5′ ^{32}P-labeled 24-mer RNA (shown at the *bottom*, with the 5′ ^{32}P label denoted by ●), and 0, 1, 2, or 4 pmol of the indicated PNPase (as monomer) were incubated for 15 min at 37 °C. The products were resolved by PAGE and visualized by autoradiography. (C) Aliquots (6 μg) of the indicated PNPase preparations were analyzed by SDS-PAGE. The Coomassie Blue-stained gel is shown. The positions and sizes (kDa) of marker polypeptides are indicated on the *left*.

Although PNPase is generally regarded as an RNA modifying enzyme, exemplary bacterial PNPases are capable of synthesizing or degrading DNA *in vitro* when manganese or iron is provided in lieu of magnesium as the metal cofactor.[9−13] Is this an *in vitro* quirk or might PNPase play a role in DNA metabolism? Recent genetic evidence implicates PNPase in bacterial DNA repair and mutagenesis *in vivo*.[12−15] Moreover, Juan Alonso and colleagues make a good case for the direct involvement of *Bacillus subtilis* PNPase in DNA repair. They document that purified *B. subtilis* PNPase catalyzes Mn^{2+}-dependent 3′ phosphorolysis of single-stranded (ss) DNA and Mn^{2+}-dependent, template-independent polymerization of dADP at the 3′-OH terminus of a ssDNA primer.[12,13] They provide genetic evidence (via studies of the effects of a Δ*pnpA* null allele on clastogen sensitivity and its epistasis relationships to null alleles of other DNA repair factors) that PNPase participates in the homologous recombination (HR) and nonhomologous end joining (NHEJ) pathways of *B. subtilis* double-strand break (DSB) repair in response to damage by hydrogen peroxide.[12] And they show that Δ*pnpA* cells do not differ from wild-type cells with respect to the levels of RNA transcripts derived from genes involved in DNA repair and recombination.[12] Although the mechanisms by which PNPase affects DNA repair are not yet clear, Alonso and colleagues suggest that PNPase reacts with broken DNA ends, either converting them from nonligatable "dirty" breaks to clean ends that can be sealed by DNA ligase or by adding nontemplated single-stranded 3′ tails that can then influence repair pathway choice.[12,13]

These studies of *Bacillus* PNPase prompted our interest in the DNA end modifying capacity of PNPase from mycobacteria, a genus of *Actinobacteria* that includes the human pathogen *M. tuberculosis* and its avirulent cousin *M. smegmatis*. Mycobacteria elaborate three genetically distinct pathways for the repair of DNA double-strand breaks: HR, NHEJ, and single-strand annealing.[16] The *M. smegmatis* HR pathway comprises parallel RecA-dependent branches, one that relies on the AdnAB helicase-nuclease and a second that relies on RecO.[16,17] (This is similar to the situation in *B. subtilis*, which has AddAB- and RecO-driven branches of RecA-dependent HR *in vivo*.[18]) The mycobacterial NHEJ system has been studied extensively *in vivo* and *in vitro*.[19] The core components are the DNA end-binding protein Ku and DNA ligases D and C. Mycobacterial NHEJ at blunt and 5′-overhang DSBs is highly mutagenic, because nucleotides are added or subtracted from the broken ends prior to their sealing by ligase.[20,21] At least some of these end-remodeling reactions are performed by LigD, which is a multifunctional enzyme composed of three

dx.doi.org/10.1021/bi400281w | *Biochemistry* 2013, 52, 2967−2981

autonomous catalytic modules — ligase (LIG), polymerase (POL) and 3′-phosphoesterase (PE) — fused into a single polypeptide.[21−25] The polymerase and 3′-phosphoesterase activities of bacterial LigD are dependent on manganese,[26−28] and the ligase activities of LigD and LigC prefer manganese to magnesium.[28]

Here, we purified and characterized recombinant *M. smegmatis* PNPase and gauged the effects of active site mutations and domain deletions. As expected, we find that the full-length *M. smegmatis* PNPase is a homotrimeric enzyme with Mg^{2+}•PO_4-dependent RNA 3′-phosphorylase and Mg^{2+}•ADP-dependent RNA polymerase activities. We show that the enzyme is a Mn^{2+}•dADP-dependent template-independent DNA polymerase and a Mn^{2+}•PO_4-dependent DNA 3′-phosphorylase. Whereas serial subtraction of the S1 and KH domains incrementally suppresses the RNA-dependent activities of mycobacterial PNPase, the DNA polymerase and DNA phosphorylase activities are stimulated by deletion of the S1 domain. A PNPase that lacks the S1 and KH domains is as active in DNA synthesis and more active in DNA phosphorolysis than the full-length enzyme. These studies suggest that the S1 and KH domains act as RNA specificity filters for mycobacterial PNPase.

EXPERIMENTAL PROCEDURES

Expression Vectors for *M. smegmatis* PNPase. The Msmeg_2656 ORF encoding the 763-aa PNPase polypeptide was PCR-amplified from *M. smegmatis* genomic DNA with primers designed to introduce NdeI sites at the start codon and 3′ of the stop codon. Truncated variants PNPase-(1−656) lacking the S1 domain (Δ*S1*) and PNPase-(1−591) lacking the KH and S1 domains (Δ*S1*+ΔKH) were amplified using antisense primers that introduced internal stop codons and a flanking Nde1 site. The putative metal-binding Asp526 residue was changed to alanine in the context of full-length PNPase and the Δ*S1* variant by PCR using mutagenic primers. The PCR products were digested with NdeI and inserted into pET16b to generate pET16b-*Msm*PNPase plasmids in which the PNPase polypeptide was fused to an N-terminal His_{10} tag. The inserts were sequenced completely to exclude the acquisition of unwanted changes during amplification and cloning.

Purification of *M. smegmatis* PNPase. The pET-*Msm*PNPase plasmids were transformed into *Escherichia coli* BL21(DE3). Cultures (1 L) of *E. coli* BL21(DE3)/pET16b-*Msm*PNPase were grown at 37 °C in Luria−Bertani medium containing 0.1 mg/mL ampicillin until the A_{600} reached 0.6. The cultures were chilled on ice, adjusted to 0.5 mM isopropyl-ß-D-thiogalactopyranoside and 2% (v/v) ethanol, and then incubated at 17 °C for 20 h with constant shaking. Cells were harvested by centrifugation, and the pellets were stored at −80 °C. All subsequent procedures were performed at 4 °C. Thawed bacteria were resuspended in 25 mL of lysis buffer (50 mM Tris-HCl, pH 8.0, 250 mM NaCl, 10% sucrose, 0.05% Triton X-100) and then sonicated for 5 min to achieve lysis. Insoluble material was removed by centrifugation at 16000 rpm in a Sorval SS34 rotor. The supernatants were applied to 10-mL columns of Ni^{2+}-nitrilotriacetic acid-agarose (Qiagen) that had been equilibrated with buffer A (50 mM Tris-HCl, pH 8.0, 250 mM NaCl, 10% glycerol, 0.05% Triton X-100). The columns were washed with buffer A and then eluted stepwise with buffer A containing 20, 100, 200, and 1000 mM imidazole. The polypeptide compositions of the fractions were monitored by SDS-PAGE. The PNPase proteins were recovered predominantly in the 200 mM imidazole eluate fractions, which were then dialyzed overnight against buffer B (50 mM Tris-HCl, pH 8.0, 250 mM NaCl, 10% glycerol). The dialysates were applied to 2-mL DEAE-Sephacel columns that had been equilibrated with buffer B, and the PNPase proteins were recovered in the flow-through fractions. The PNPase preparations were concentrated by centrifugal ultrafiltration to ∼15 mg/mL, then adjusted to 2 mM EDTA, and gel-filtered through a column of Superdex-200 equilibrated in 20 mM Tris pH 8.0, 100 mM NaCl, 10% glycerol. The peak fractions were pooled, concentrated by centrifugal ultrafiltration, and stored at −80 °C. Protein concentrations were determined by using the Bio-Rad dye reagent with BSA as the standard.

RNA 3′-Phosphorylase Assay. A synthetic 24-mer RNA was 5′-radiolabeled by using T4 polynucleotide kinase and [γ-^{32}P]ATP and then purified by electrophoresis through a native 18% polyacrylamide gel. RNA phosphorylase reaction mixtures (10 μL) containing 20 mM Tris-HCl (pH 7.5), 5 mM $MgCl_2$, 0.5 mM $(NH_4)_2PO_4$, 1 pmol (0.1 μM) of 5′ ^{32}P-labeled 24-mer RNA and PNPase as specified (expressed as pmol of PNPase monomer) were incubated for 15 min at 37 °C. The reactions were quenched by adding 10 μL of 90% formamide, 50 mM EDTA. The samples were heated for 5 min at 100 °C and then analyzed by electrophoresis through a 40-cm 20% polyacrylamide gel containing 7.5 M urea in 44.5 mM Tris-borate (pH 8.3), 1 mM EDTA. The radiolabeled RNAs were visualized by autoradiography.

RNA Polymerase Assay. Reaction mixtures (10 μL) containing 20 mM Tris-HCl (pH 7.5), 5 mM $MgCl_2$, 2 mM ADP, 1 pmol (0.1 μM) 5′ ^{32}P-labeled 24-mer RNA primer, and PNPase as specified were incubated at 37 °C for 15 min. The reactions were quenched by adding 10 μL of 90% formamide, 50 mM EDTA. The samples were heated for 5 min at 100 °C and then analyzed by electrophoresis through a 40-cm 12% polyacrylamide gel containing 7.5 M urea in 44.5 mM Tris-borate (pH 8.3), 1 mM EDTA. The radiolabeled RNAs were visualized by autoradiography.

DNA Polymerase Assay. A synthetic 24-mer DNA was 5′-radiolabeled by using T4 polynucleotide kinase and [γ-^{32}P]ATP and then purified by electrophoresis through a native 18% polyacrylamide gel. DNA polymerase reaction mixtures (10 μL) containing 20 mM Tris-HCl (pH 7.5), 5 or 10 mM $MnCl_2$, 2 mM dADP, 1 pmol (0.1 μM) 5′ ^{32}P-labeled 24-mer DNA primer, and PNPase as specified were incubated for 30 min at 37 °C. The reactions were quenched by adding 10 μL of 90% formamide, 50 mM EDTA. The samples were heated for 5 min at 100 °C and then analyzed by electrophoresis through a 40-cm 12% polyacrylamide gel containing 7.5 M urea in 44.5 mM Tris-borate (pH 8.3), 1 mM EDTA. The radiolabeled DNAs were visualized by autoradiography.

DNA 3′-Phosphorylase Assay. Reaction mixtures (10 μL) containing 20 mM Tris-HCl (pH 7.5), 5 mM $MnCl_2$, 30 μM $(NH_4)_2PO_4$, 0.1 μM (1 pmol) of 5′ ^{32}P-labeled 24-mer DNA, and PNPase as specified were incubated for 60 min at 37 °C. The reactions were quenched by adding 10 μL of 90% formamide, 50 mM EDTA. The samples were heated for 5 min at 100 °C and then analyzed by electrophoresis through a 40-cm 14% polyacrylamide gel containing 7.5 M urea in 44.5 mM Tris-borate (pH 8.3), 1 mM EDTA. The radiolabeled DNAs were visualized by autoradiography.

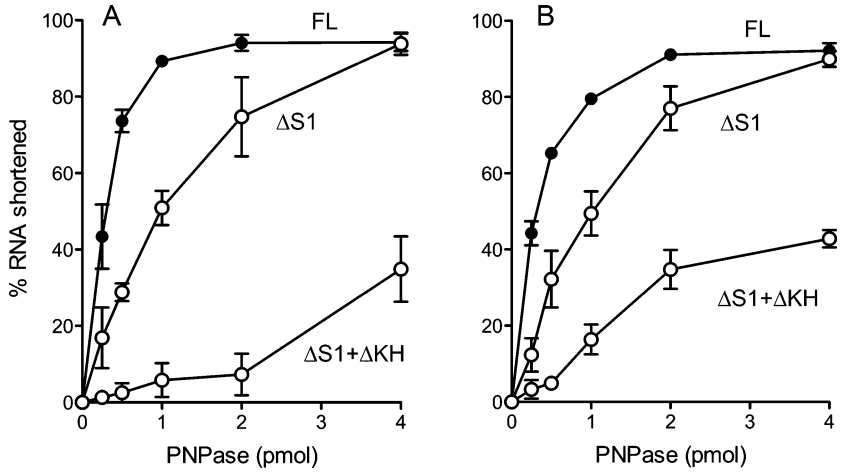

Figure 2. Effects of domain deletions on RNA phosphorylase activity. (A) Reaction mixtures (10 μL) containing 20 mM Tris-HCl (pH 7.5), 5 mM $MgCl_2$, 0.5 mM $(NH_4)_2PO_4$, 0.1 μM (1 pmol) 5′ ^{32}P-labeled 24-mer RNA, and 0, 0.25, 0.5, 1, 2, or 4 pmol (as monomer) of the indicated PNPase were incubated for 15 min at 37 °C. The products were analyzed by denaturing PAGE as in Figure 1. The unreacted RNA and the shorter products of phosphorolysis (irrespective of their size) were quantified by scanning the gel with a Fujix BAS2500 imager. The percent of RNA shortened is plotted as a function of input PNPase. Each datum in the graph is the average of four (FL and ΔS1+ΔKH) or three (ΔS1) separate enzyme titration experiments ± SEM. (B) Reaction mixtures (10 μL) containing 20 mM Tris-HCl (pH 7.5), 5 mM $MnCl_2$, 15 μM $(NH_4)_2PO_4$, 0.1 μM (1 pmol) 5′ ^{32}P-labeled 24-mer RNA, and 0, 0.25, 0.5, 1, 2, and 4 pmol of the indicated PNPase were incubated for 15 min at 37 °C. The products were analyzed by denaturing PAGE, and the unreacted RNA and shorter products of phosphorolysis were quantified by scanning the gel. The percent of RNA shortened is plotted as a function of input PNPase. Each datum in the graph is the average of four (FL and ΔS1) or three (ΔS1+ΔKH) separate enzyme titration experiments ± SEM. Specific activities were calculated from the slopes of the titration curves in the linear range of enzyme dependence, as determined by linear regression curve fitting in Prism.

RESULTS

RNA Phosphorylase Activity of Mycobacterial PNPase. *M. smegmatis* PNPase is a 763-aa polypeptide encoded by the Msmeg_2656 gene. Its primary structure is 87% identical to that of the 756-aa *M. tuberculosis* PNPase encoded by gene Rv2783c and 72% identical to that of *Streptomyces antibioticus* PNPase (757-aa), the first PNPase for which a crystal structure[2] was solved, and 45% identical to *Caulobacter crescentus* PNPase (712-aa), the tertiary structure of which[6] is shown in Figure 1A. To query the biochemistry of *M. smegmatis* PNPase, we produced the full-length protein and truncated variants ΔS1 (aa 1−656) and ΔS1+ΔKH (aa 1−591) in *E. coli* as His_{10}-tagged derivatives and purified the recombinant proteins from soluble bacterial extracts by sequential nickel-affinity, anion-exchange, and gel-filtration chromatography steps. The placement of stop codons to cleanly delete the S1 and KH modules in *M. smegmatis* PNPase was guided by the crystal structure of the full-length *Caulobacter* protein.[6] SDS-PAGE showed that the full-length (FL) *M. smegmatis* PNPase preparation comprised a predominant polypeptide consistent with the predicted size of the recombinant protein (84 kDa), whereas the ΔS1 and ΔS1+ΔKH preparations comprised polypeptides that migrated incrementally faster, as expected (Figure 1C).

To test the mycobacterial PNPases for RNA phosphorylase activity, we reacted them for 15 min with a 5′ ^{32}P-labeled 24-mer RNA (1 pmol) in the presence of 5 mM Mg^{2+} and 0.5 mM phosphate. The reaction products were analyzed by urea-PAGE and the labeled RNAs visualized by autoradiography (Figure 1B). We saw that 1 pmol of full-length PNPase protomer sufficed to convert most of the input 24-mer RNA to a mixture of trinucleotide and mononucleotide end-products (Figure 1B, FL). The ΔS1 PNPase displayed lower activity than the full-length enzyme; i.e., there was scant RNA decay elicited by 1 pmol of input ΔS1, which increased at 2 pmol and sufficed at 4 pmol to convert most of the input 24-mer to a radiolabeled mononucleotide end-product (Figure 1B, ΔS1). Because we did not see significant accumulation of decay intermediates at limiting ΔS1 levels, we infer that the loss of the S1 domain did not compromise phosphorylase processivity, but rather that the S1 domain contributes to the initial formation of a productive PNPase•RNA complex, as suggested for *E. coli* PNPase.[8] Simultaneous deletion of the S1 and KH domains caused a more severe defect in RNA decay, whereby we saw no phosphorylase activity at 1 and 2 pmol of input ΔS1+ΔKH protein and 4 pmol elicited scant trimming of 1−4 nucleotides from the 3′ end and scant formation of 5′-labeled trinucleotide and mononucleotide products (Figure 1B, ΔS1+ΔKH). To gauge phosphorylase specific activity, we back-titrated the enzymes to establish a linear response range for the full-length PNPase and quantified the activity as the percent of the input ^{32}P-labeled 24-mer converted to shorter fragments (irrespective of the size of the decay products). The results (Figure 2A) showed that the Mg^{2+}-dependent RNA phosphorylase specific activities of the ΔS1 and ΔS1+ΔKH PNPases (calculated from the slopes of the titration curves in the linear range of enzyme dependence, as determined by linear regression curve fitting in Prism) were 3-fold less and 20-fold less than that of full-length PNPase, respectively.

Requirements for RNA Phosphorylase Activity. To verify that the observed RNA decay activity was intrinsic to the recombinant PNPase proteins, we mutated the predicted binding site for the metal cofactor. The crystal structure of *E. coli* PNPase in complex with Mn^{2+} had identified Asp486 and Asp492 within the peptide ^{486}**D**HLGDM**D**^{492} as direct metal ligands.[4] The equivalent motif in the distal PH domain of *M. smegmatis* PNPase is ^{526}**D**AFGDM**D**^{532} (Figure 1A). Whereas it has been shown that replacing the distal metal-binding Asp492 residue of *E. coli* PNPase with glycine abolished phosphorylase activity,[7] as did the equivalent Asp-to-Gly mutation of *Bacillus*

dx.doi.org/10.1021/bi400281w | *Biochemistry* 2013, 52, 2967−2981

PNPase,[13] to our knowledge there has been no report of the effects of subtracting the other metal-binding aspartate. Therefore, we introduced a D526A mutation into the full-length and ΔS1 mycobacterial PNPases and tested the purified FL-D526A and ΔS1-D526A mutant proteins (Figure 1C) for RNA phosphorylase activity (Figure 1B). The D526A mutants failed to convert the 24-mer RNA to trinucleotide and mononucleotide products at 4 pmol of input protein, a level sufficient for virtually complete phosphorolysis by the Asp526-containing full-length and ΔS1 enzymes (Figure 1B). The D526A preparations performed only scant trimming of 1−4 nucleotides from the RNA 3′ end (Figure 1B). These results affirm that the phosphorylase activity inheres to the mycobacterial PNPase and they attest to the essentiality of the metal-binding Asp526 residue. Additional controls verified that the RNA phosphorylase activity of ΔS1 PNPase depended on exogenous phosphate and Mg^{2+}, with optimal activity at 0.5 mM phosphate (not shown).

Manganese could replace magnesium as the cofactor for the RNA phosphorylase activity. Mn^{2+}-dependent RNA phosphorylase was optimal at 15−30 μM phosphate and inhibited at ≥250 μM phosphate (not shown). The specific activity of full-length PNPase as a Mn^{2+}-dependent RNA phosphorylase was similar to its specific activity as a Mg^{2+}-dependent RNA phosphorylase (compare Figure 2A,B). The Mn^{2+}-dependent RNA phosphorylase specific activities of the ΔS1 and ΔS1+ΔKH PNPases were 3-fold less and 10-fold less than that of full-length PNPase, respectively (Figure 2B).

RNA Polymerase Activity of *M. smegmatis* PNPase. When the 5′ ^{32}P-labeled 24-mer RNA was reacted with full-length PNPase in the presence of 5 mM Mg^{2+} and 2 mM ADP (in lieu of phosphate), the enzyme switched to its polymerase mode, such that the labeled RNA strand served as a primer for addition of a poly(A) tail (Figure 3, FL). The fraction of input primers extended increased in proportion to the level of input full-length PNPase; the product size distribution after a 15 min reaction appeared bimodal, with a population of extended RNAs centered about ∼60 nucleotides plus a population with very long tails that migrated slowly and were not well resolved. The truncated ΔS1 protein retained RNA polymerase activity, albeit less than full-length PNPase, as gauged by the fraction of input RNA primer extended at equivalent enzyme levels (Figure 3, ΔS1). Nonetheless, the ΔS1 reaction products had very long poly(A) tails, suggesting that processivity was intact. These results fortify the inferences from the phosphorylase assays that the S1 domain promotes the productive engagement of the RNA strand. Simultaneous deletion of the S1 and KH domains caused a further decrement in PNPase RNA polymerase activity, with respect to inefficient primer utilization and the appearance of a subpopulation of products extended by 15−20 adenylates along with those that had very long tails (Figure 3, ΔS1+ΔKH). As a gauge of polymerase activity, we quantified the percent of the input ^{32}P-labeled 24-mer extended by 1 or more AMP additions. The results (Figure 4A) showed that the Mg^{2+}-dependent RNA polymerase specific activities of the ΔS1 and ΔS1+ΔKH PNPases (calculated from the slopes of the titration curves in the linear range of enzyme dependence, by linear regression curve fitting in Prism) were 3.7-fold less and 13-fold less than that of full-length PNPase, respectively.

Mycobacterial PNPase Is a Homotrimer. To verify that the phosphorylase and polymerase are native to the mycobacterial PNPase, we analyzed the full-length protein by zonal velocity sedimentation through a 15−30% glycerol gradient. SDS-PAGE analysis of the gradient fractions (Figure 5A) showed that the 84 kDa PNPase polypeptide sedimented as a relatively discrete peak in fractions 11−13. Comparison to the peak positions of marker proteins BSA (native size 66 kDa) and catalase (native size 256 kDa) sedimented in a parallel gradient — and denoted by arrows in Figure 5A — indicated that mycobacterial PNPase is a homotrimer in solution, as expected. Surveying the gradient fractions for RNA phosphorylase activity showed a peak centered around fractions 11−13 (Figure 5B). Similarly, the RNA polymerase activity peaked in fractions 11−13 (Figure 5C).

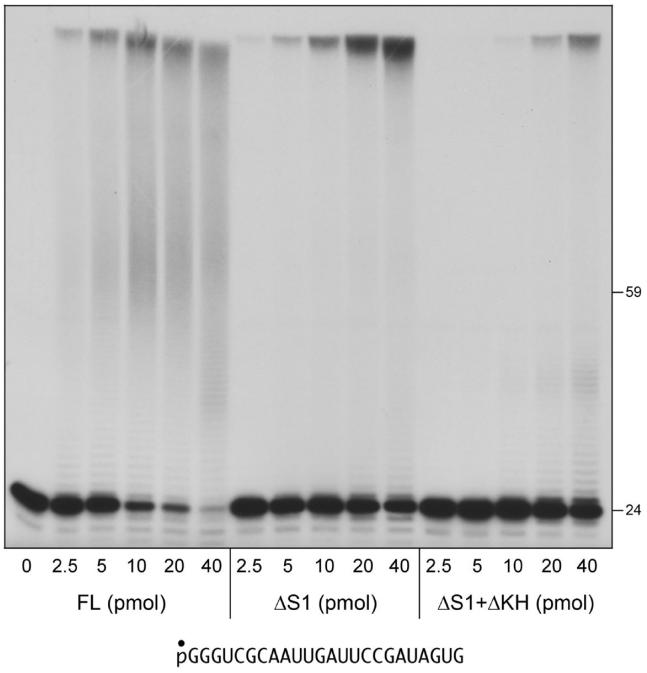

Figure 3. RNA polymerase activity of mycobacterial PNPase. Reaction mixtures (10 μL) containing 20 mM Tris-HCl (pH 7.5), 5 mM $MgCl_2$, 2 mM ADP, 1 pmol (0.1 μM) of 5′ ^{32}P-labeled 24-mer RNA primer (depicted at *bottom*), and full-length (FL) PNPase or truncated versions ΔS1 or ΔS1+ΔKH as specified (expressed as pmol of monomer) were incubated for 15 min at 37 °C. The products were resolved by PAGE and visualized by autoradiography. The positions of the 24-mer primer and a 5′-labeled 59-mer marker oligonucleotide are indicated at *right*.

Mycobacterial PNPase Is a Manganese-Dependent DNA Polymerase. Full-length PNPase catalyzed nontemplated DNA synthesis, as gauged by its ability, in the presence of 5 mM Mn^{2+} and 2 mM dADP, to extend a 5′ ^{32}P-labeled 24-mer DNA primer strand (Figure 6A). dAMP addition yielded a ladder of radiolabeled products with a bimodal size distribution. At limiting PNPase levels, the primers were extended by 1−8 nucleotides; higher enzyme levels led to the appearance of a cluster of longer products (∼50−80 nucleotides). DNA synthesis by full-length PNPase was abolished by the D526A mutation (Figure 6B), suggesting that the same metal-binding site accommodates Mg^{2+} for RNA transactions and Mn^{2+} for DNA polymerization. In the absence of exogenous dADP, full-length PNPase generated a cluster of short extension products (25−30 nucleotides) (Figures 6B and S1). We attribute this limited synthesis to the presence of enzyme-bound nucleoside diphosphates in the recombinant PNPase preparation. Note that the A_{260}/A_{280} ratio of the gel-filtered full-length PNPase

dx.doi.org/10.1021/bi400281w | *Biochemistry* 2013, 52, 2967−2981

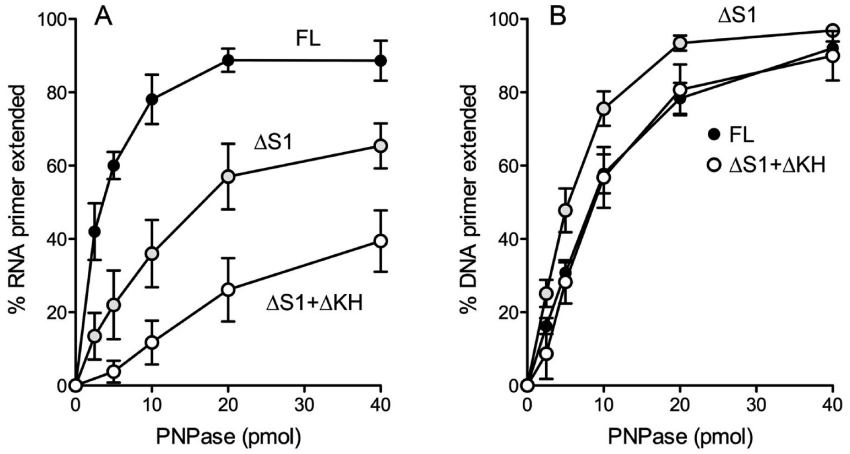

Figure 4. Effects of domain deletions of RNA and DNA polymerase activity. (A) RNA polymerase. Reaction mixtures (10 μL) containing 20 mM Tris-HCl (pH 7.5), 5 mM $MgCl_2$, 2 mM ADP, 1 pmol of 5′ ^{32}P-labeled 24-mer RNA primer, and full-length (FL), Δ*S*1 or Δ*S*1+ΔKH PNPase as specified were incubated for 15 min at 37 °C. The products were resolved by PAGE. The unreacted RNA and the longer products of AMP addition (collectively, irrespective of their size) were quantified by scanning the gel. The percent of the RNA primer extended is plotted as a function of input PNPase (pmol of monomer). Each datum in the graph is the average of three separate enzyme titration experiments ± SEM (B) DNA polymerase. Reaction mixtures (10 μL) containing 20 mM Tris-HCl (pH 7.5), 5 mM $MnCl_2$, 2 mM dADP, 1 pmol of 5′ ^{32}P-labeled 24-mer DNA primer (see Figure 6A) and full-length (FL), Δ*S*1 or Δ*S*1+ΔKH PNPase or as specified were incubated for 30 min at 37 °C. The unreacted DNA and the longer products of dAMP addition (collectively, irrespective of their size) were quantified by scanning the gel. The percent of the DNA primer extended is plotted as a function of input PNPase. Each datum in the graph is the average of six (FL and Δ*S*1) or three (Δ*S*1+ΔKH) separate enzyme titration experiments ± SEM. Specific activities were calculated from the slopes of the titration curves in the linear range of enzyme dependence, as determined by linear regression curve fitting in Prism.

was 1.4, which is significantly higher than the value of 0.57 expected for pure protein, consistent with nucleotides and/or nucleic acid copurifying with the full-length mycobacterial PNPase. (Copurification of RNA with full-length recombinant *Streptomyces* and *Caulobacter* PNPases produced in *E. coli* was described previously by Luisi and colleagues.[2,6])

Deletion of the S1 Domain Stimulates DNA Polymerase Activity. To our surprise, the Δ*S*1 PNPase was more active as a DNA polymerase than full-length PNPase (Figure 6A). The efficiency of DNA primer utilization by Δ*S*1 as a function of input enzyme (defined as the percent of primer extended by one or more dAMP additions) was 60% higher than full-length PNPase, as gauged by the slope of the titration curve in the linear range of enzyme dependence (Figure 4B). Moreover, the extended primers at limiting and saturating Δ*S*1 were predominantly the cluster of 50−80 nucleotide DNAs, without the short extension products generated by full-length PNPase (Figure 6A). DNA synthesis by Δ*S*1 was abolished by the D526A mutation (Figure 6B). When dADP was omitted, the Δ*S*1 enzyme extended the DNA primer by 1−5 nucleotides (Figure 6B and S1). Here again, we invoke the presence of enzyme-bound nucleoside diphosphates in the Δ*S*1 preparation. Our observation that the A_{260}/A_{280} ratio of the gel-filtered Δ*S*1 enzyme was 0.78 (i.e., lower than that of full-length PNPase, but still higher than expected for pure protein) suggested that less RNA copurified with the enzyme when the S1 domain was missing.

Also surprising was the finding that the Δ*S*1+ΔKH variant was as active as full-length PNPase with respect to DNA synthesis. Whereas the efficiency of DNA primer utilization by Δ*S*1+ΔKH as a function of enzyme was virtually identical to that of full-length PNPase (Figure 4B), the Δ*S*1+ΔKH enzyme (like Δ*S*1) did not accumulate the short extension products seen with full-length PNPase, but instead generated a cluster of DNAs ∼35−60 nucleotides long, slightly shorter than the cluster synthesized by Δ*S*1 (Figure 6A). When dADP was omitted, the Δ*S*1+ΔKH enzyme extended a minor fraction of the input DNA primers by only one nucleotide (Figure S1). Apparently, the Δ*S*1+ΔKH protein had a lower level of prebound NDPs than did the FL and Δ*S*1 PNPases. Indeed, the A_{260}/A_{280} ratio of the gel-filtered Δ*S*1+ΔKH enzyme was 0.59, indicating that deletion of the S1 and KH domains also resulted in minimal RNA copurification with the mycobacterial PNPase. This is consistent with the apparent absence of enzyme-bound RNA in recombinant *E. coli* PNPase lacking the KH and S1 modules.[4]

To gauge whether the endogenous nucleotides added to the DNA primer terminus by the full-length and Δ*S*1 PNPases were ribonucleotides or deoxyribonucleotides, we treated the reaction products with NaOH. The reaction mixtures were adjusted to 0.15 M NaOH and incubated overnight at 37 °C, then neutralized with HCl and analyzed by urea-PAGE. Any −rNpX− phosphodiesters in the radiolabeled product strands will be hydrolyzed in alkali to yield a mixture of −rN3′p and −rN2′p terminated chains, whereas −dNpX linkages will be stable in alkali. Control experiments showed that the 5′ ^{32}P-labeled DNA primer was alkali-stable, as expected. We found that the cluster of short extension products synthesized by full-length PNPase was alkali-sensitive, i.e., reduced to a species one nucleotide longer that the input ssDNA after NaOH treatment (not shown), thus signifying that the enzyme contained prebound rNDPs. The cluster of short extension products generated by the Δ*S*1 PNPase was also alkali-sensitive (not shown). By contrast, the longer chains synthesized in the presence of added dADP were alkali-stable (not shown), thereby verifying that the PNPase is a *bona fide* DNA polymerase.

Domain Deletions Stimulate a DNA Phosphorylase Activity. We tested the PNPase proteins (20 pmol) for their ability to resect the 3′ end of a 5′ ^{32}P-labeled ssDNA substrate. Reaction mixtures containing 24-mer ssDNA (1 pmol), 20 pmol of PNPase protomer, 5 mM Mn^{2+}, and 30 μM inorganic

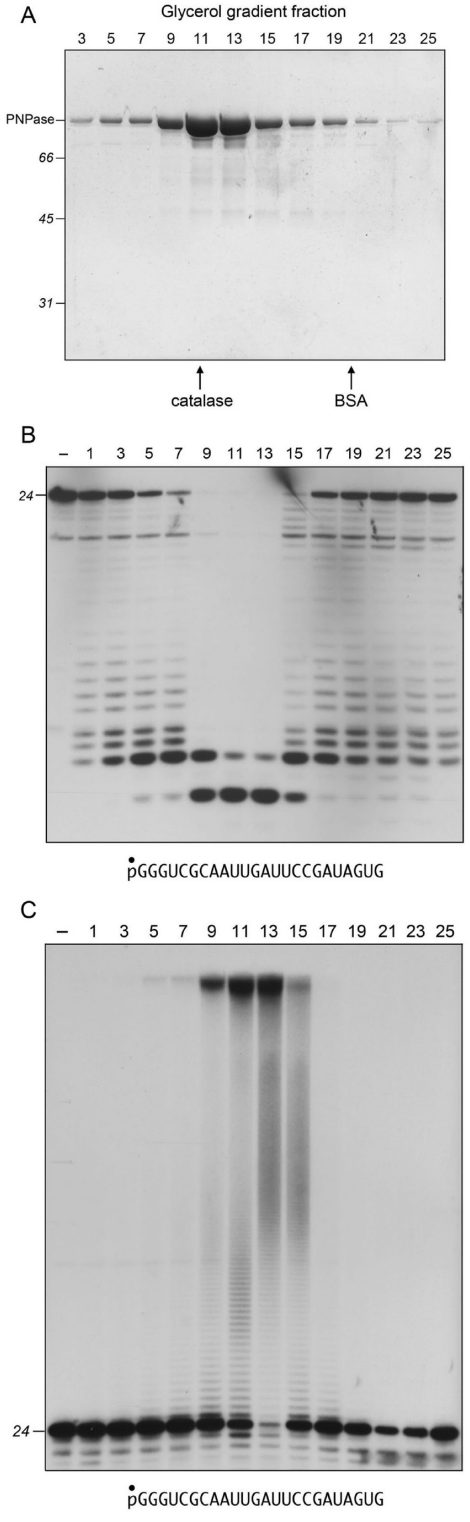

Figure 5. PNPase sediments as a homotrimer. Full-length PNPase (0.66 mg in 0.2 mL) was applied to a 4.8-mL 15–30% glycerol gradient containing 50 mM Tris-HCl (pH 8.0), 250 mM NaCl, 1 mM EDTA, 0.05% Triton X-100. A mixture of catalase (50 μg) and BSA (50 μg) was applied to a second glycerol gradient prepared in parallel. The gradients were centrifuged at 50 000 rpm for 11.5 h at 4 °C in a Beckman SW55Ti rotor. Fractions (0.2 mL) were collected from the bottoms of the tubes. (A) Aliquots (20 μL) of the odd-numbered fractions from the PNPase glycerol gradient were analyzed by SDS-PAGE. The Coomassie Blue-stained gel is shown. Positions and sizes (kDa) of marker polypeptides are indicated at left. The sedimentation peaks of catalase (native size 256 kDa) and BSA (native size 66 kDa) that were analyzed in a parallel gradient are indicated by vertical arrows at *bottom*. (B) RNA phosphorylase reaction mixtures (10 μL) containing 20 mM Tris-HCl (pH 7.5), 5 mM $MgCl_2$, 0.5 mM ammonium phosphate, 1 pmol of 5′ ^{32}P-labeled 24-mer RNA substrate (depicted at bottom), and 1 μL of the indicated glycerol gradient fraction were incubated for 5 min at 37 °C. (C) RNA polymerase reaction mixtures (20 μL) containing 20 mM Tris-HCl (pH 7.5), 5 mM $MgCl_2$, 2 mM ADP, 1 pmol of 5′ ^{32}P-labeled 24-mer RNA primer, and 1 μL of the indicated glycerol gradient fractions were incubated for 30 min at 37 °C. The phosphorylase and polymerase reaction products were analyzed by PAGE and visualized by autoradiography.

phosphate were incubated for 60 min at 37 °C; reactions lacking exogenous phosphate were included as controls (Figure S1). For full-length wild-type PNPase, the inclusion of phosphate diminished the addition of endogenous NDPs beyond the first step, while eliciting the appearance of ^{32}P-labeled decay products shorter than the input 24-mer. For Δ*S*1 PNPase, the inclusion of phosphate suppressed the endogenous NDP additions, while promoting a higher level of DNA phosphorylase activity that that seen for full-length PNPase, as gauged by the fraction of the input substrates shortened by one or more nucleotides (which was 61%) and the smaller sizes of the resected strands. The DNA phosphorylase activities of the full-length and Δ*S*1 PNPase enzymes were effaced by the D526A mutation (Figure S1), verifying that the resection activities were intrinsic to PNPase. The Δ*S*1+ΔKH enzyme was more active in phosphate-dependent DNA end resection (81% of the input strands shortened) than either the full-length or Δ*S*1 proteins (Figure S1).

Taken together, the experiments reveal that the deletion of the S1 domain exerts opposite effects on DNA polymerization and DNA phosphorylase (increased activity) versus RNA polymerization and RNA decay (decreased activity). Moreover, the disparity between residual DNA and RNA activities is amplified when the S1 and KH domains are deleted simultaneously. We infer that the S1 and KH domains of mycobacterial PNPase confer selectivity for RNA transactions.

Effects of Domain Deletion on Binding of Mycobacterial PNPase to RNA and DNA. We implemented an electrophoretic mobility shift assay to study the binding of PNPase to the 5′ ^{32}P-labeled 24-mer RNA primer. Incubation of 40 pmol of full-length PNPase (as monomer) with 1 pmol of RNA in the absence of metal, phosphate, or ADP (to preclude the phosphorylase and polymerase activity) resulted in the formation of a discrete PNPase•RNA complex that was well resolved from free RNA during native PAGE (Figure 7A). 52% of the input RNA was associated with the full-length PNPase•RNA complex. (We construe the comet-like trail of labeled RNA above the free RNA species to indicate that a fraction of the PNPase•RNA complex dissociated during the PAGE procedure.) By contrast, the Δ*S*1 protein displayed feeble binding to the 24-mer RNA in the absence of divalent cation (only 7% of the RNA was PNPase•RNA complex) and the Δ*S*1+ΔKH protein failed to form a stable RNA complex under these conditions (Figure 7A). The results implicate the S1 domain as the principal mediator of RNA binding by mycobacterial PNPase in the absence of a divalent metal. When a 5′ ^{32}P-labeled 24-mer DNA primer was used as the nucleic acid ligand, there was minimal formation of a PNPase•DNA

dx.doi.org/10.1021/bi400281w | *Biochemistry* 2013, 52, 2967–2981

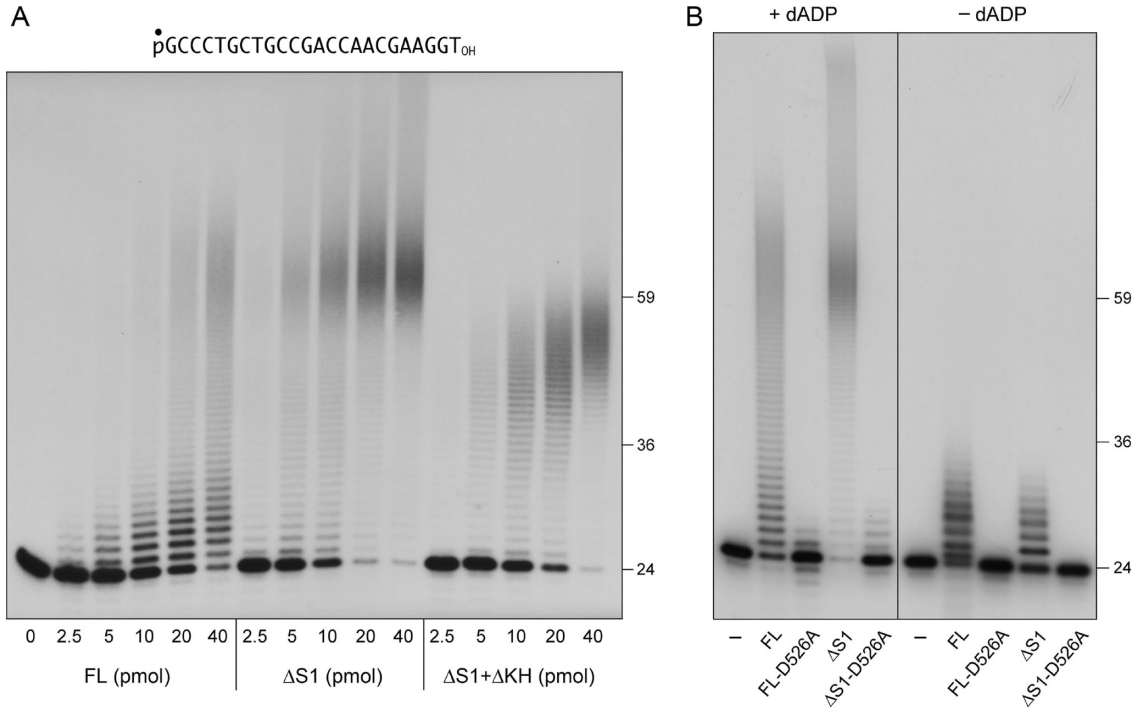

Figure 6. DNA polymerase activity of mycobacterial PNPase. (A) Reaction mixtures (10 μL) containing 20 mM Tris-HCl (pH 7.5), 5 mM $MnCl_2$, 2 mM dADP, 1 pmol (0.1 μM) of 5′ ^{32}P-labeled 24-mer DNA primer (depicted at *top*, with the 5′ ^{32}P label denoted by ●), and full-length (FL) PNPase or truncated versions Δ*S*1 or Δ*S*1+ΔKH as specified (expressed as pmol of monomer) were incubated for 30 min at 37 °C. (B) Reaction mixtures (10 μL) containing 20 mM Tris-HCl (pH 7.5), 5 mM $MnCl_2$, 1 pmol of 5′ ^{32}P-labeled 24-mer DNA substrate, 40 pmol of the indicated PNPase protein, and either 2 mM dADP (left lanes) or no dADP (right lanes) were incubated for 30 min at 37 °C. PNPase was omitted from control reactions in lanes –. The products were resolved by PAGE and visualized by autoradiography. The positions of the 24-mer primer and 5′-radiolabeled 36-mer and 59-mer marker oligonucleotides are indicated at *right*.

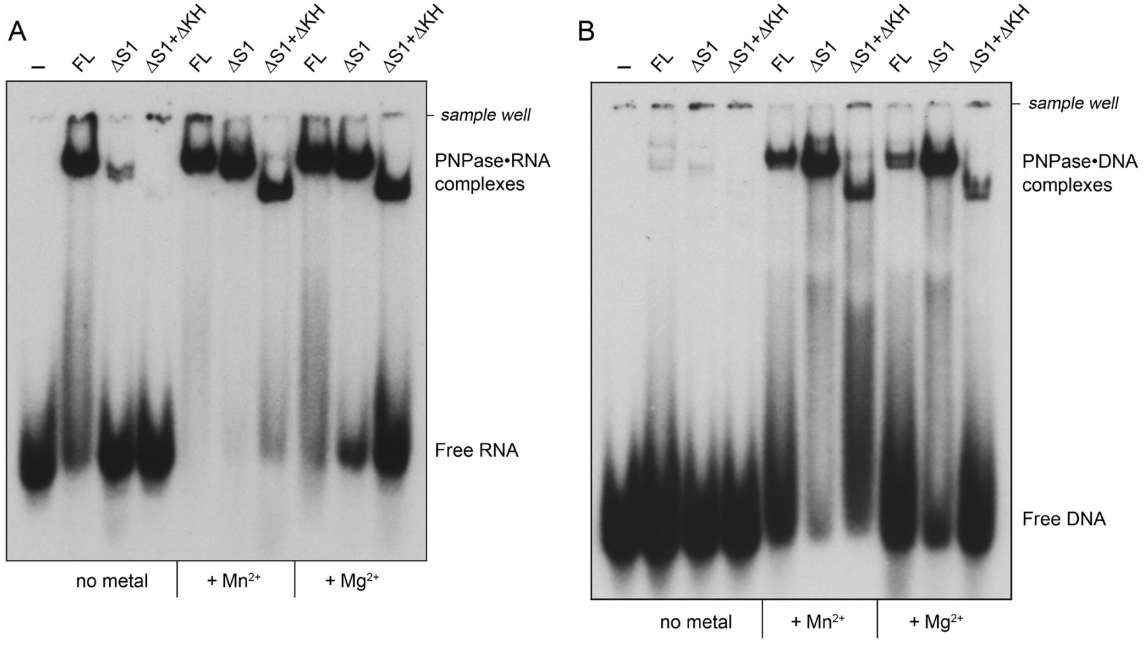

Figure 7. Gel-shift assay of RNA and DNA binding by mycobacterial PNPase. Reaction mixtures (10 μL) containing 20 mM Tris-HCl (pH 7.5), 10% glycerol, 40 pmol of the indicated PNPase (as monomer), and either no metal or 5 mM Mn^{2+} or 5 mM Mg^{2+}, and 0.1 μM (1 pmol) 5′ ^{32}P-labeled 24-mer RNA (panel A) or 24-mer DNA (panel B) were incubated for 20 min on ice. The mixtures were adjusted to 20% glycerol and then analyzed by electrophoresis through a 15-cm native 6% polyacrylamide gel containing 22.5 mM Tris-borate. The gel was run at 110 V in the cold room for 3 h and then dried under a vacuum on DE81 paper. The free ^{32}P-labeled DNA and slower migrating PNPase●[^{32}P]-nucleic acid complexes were visualized by autoradiography of the dried gel.

dx.doi.org/10.1021/bi400281w | *Biochemistry* 2013, 52, 2967–2981

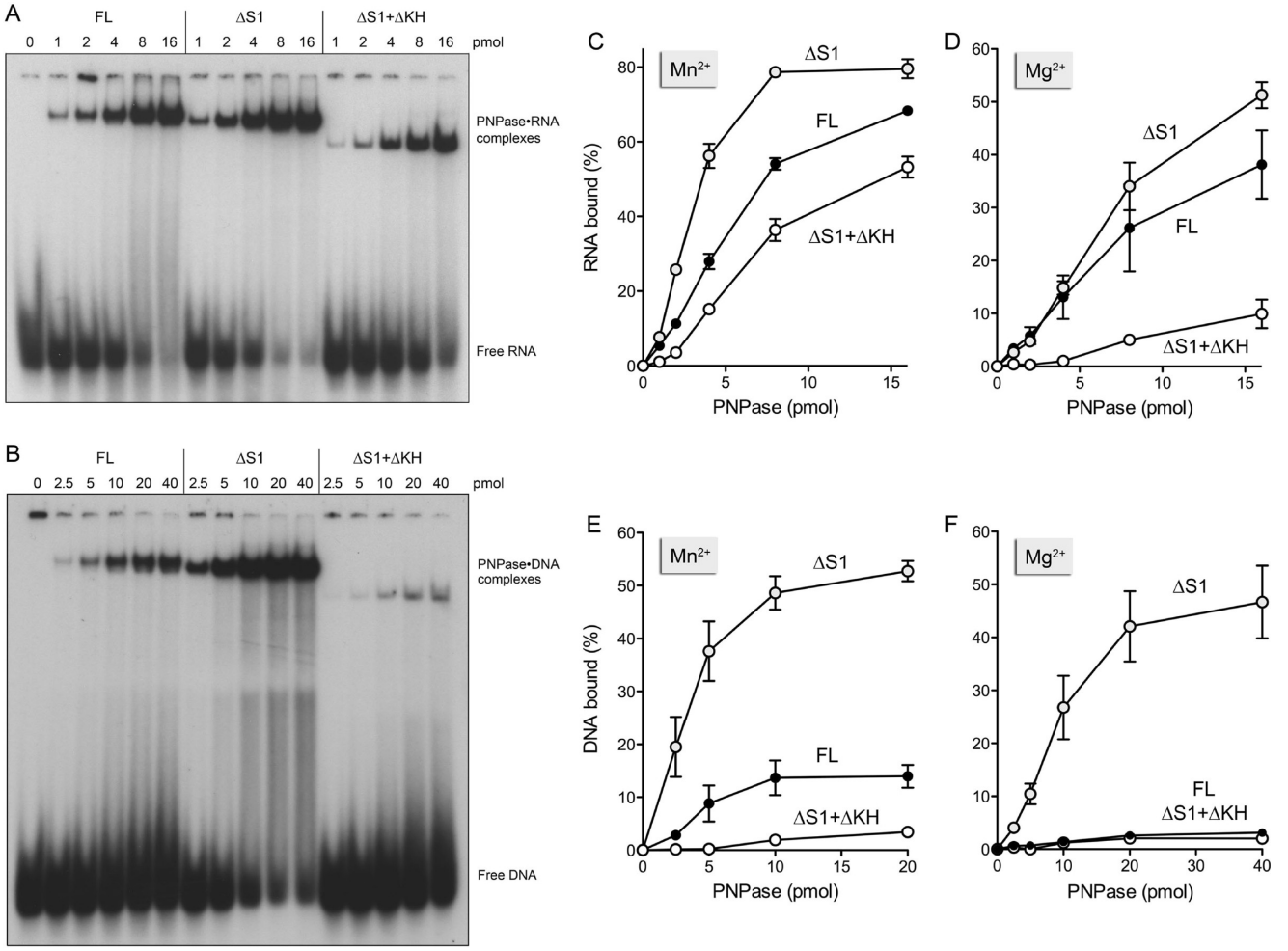

Figure 8. Effects of domain deletions on RNA and DNA binding in the presence of Mg^{2+} and Mn^{2+}. (A and B) Binding reaction mixtures (10 μL) containing 20 mM Tris-HCl (pH 7.5), 10% glycerol, 5 mM Mn^{2+}, 0.1 μM (1 pmol) 5′ ^{32}P-labeled 24-mer RNA (panel A) or 24-mer DNA (panel B), and full-length, Δ*S*1, or Δ*S*1+ΔKH PNPase as specified were incubated for 20 min on ice. The mixtures were analyzed by native PAGE as described in Figure 7; autoradiograms of the gels are shown. (C and D) RNA binding reactions contained 5 mM Mn^{2+} (panel C) or 5 mM Mg^{2+} (panel D) and PNPase proteins as specified. (E and F) DNA binding reactions contained 5 mM Mn^{2+} (panel E) or 5 mM Mg^{2+} (panel F) and PNPase proteins as specified. The mixtures were analyzed by native PAGE. The fraction of the input RNA or DNA associated with PNPase•nucleic acid complexes was quantified by scanning the gel and is plotted as a function of input PNPase. Each datum in the graphs is the average of three separate protein titration experiments ± SEM.

complex by the full-length and Δ*S*1 proteins (only 1% of the input DNA was bound) and no detectable DNA binding by Δ*S*1+ΔKH in the absence of a metal (Figure 7B). Thus, PNPase discriminates strongly between RNA and DNA at the level of metal-independent interaction via the S1 domain.

The outcomes were quite different when the RNA and DNA binding reactions were performed in the presence of 5 mM divalent cation (again, in the absence of phosphate or ADP/dADP). In binding reaction mixtures containing 5 mM Mn^{2+}, the full-length, Δ*S*1 and Δ*S*1+ΔKH proteins bound 74%, 81%, and 62% of the 24-mer RNA, respectively (Figure 7A; $+Mn^{2+}$). In the presence of 5 mM Mg^{2+}, the full-length, Δ*S*1 and Δ*S*1+ΔKH proteins bound 65%, 69%, and 35% of the 24-mer RNA, respectively (Figure 7A; $+Mg^{2+}$). Note that the Δ*S*1•RNA and Δ*S*1+ΔKH•RNA complexes migrated slightly faster than the full-length PNPase•RNA complex during native PAGE, consistent with the decrements in the mass of the respective truncated enzymes (Figure 7A). These results illuminate two distinct modes of RNA binding by mycobacterial PNPase: (i) a metal-independent RNA-protein interaction with the S1 domain, and (ii) a metal-dependent RNA interaction with the core trimeric ring structure. A striking finding was that inclusion of a divalent cation enabled the full-length, Δ*S*1 and Δ*S*1+ΔKH PNPase proteins to bind to the 24-mer DNA (Figure 7B), a capacity not evident in the absence of metals.

Protein titration experiments showed that the extent of PNPase•RNA complex formation in the presence of divalent cation was proportional to the amount of input PNPase (Figure 8A) as was the extent of PNPase•DNA complex formation (Figure 8B). Quantification of the extents of RNA and DNA binding as a function of full-length, Δ*S*1, and Δ*S*1+ΔKH protein in the presence of Mg^{2+} or Mn^{2+} is shown in Figure 8 (panels C–F). We gauged the relative RNA binding activities from the slopes of the binding titration curves in the linear response range. The following themes emerged. RNA binding by each of the PNPase proteins was higher in the presence of Mn^{2+} than Mg^{2+} (Figure 8C,D). In Mn^{2+}, Δ*S*1 bound RNA 2-fold better than full-length PNPase, while Δ*S*1+ΔKH bound 80% as well as full-length PNPase (Figure 8C). In Mg^{2+}, Δ*S*1 and full-length PNPase bound RNA similarly, while Δ*S*1+ΔKH

dx.doi.org/10.1021/bi400281w | *Biochemistry* 2013, 52, 2967–2981

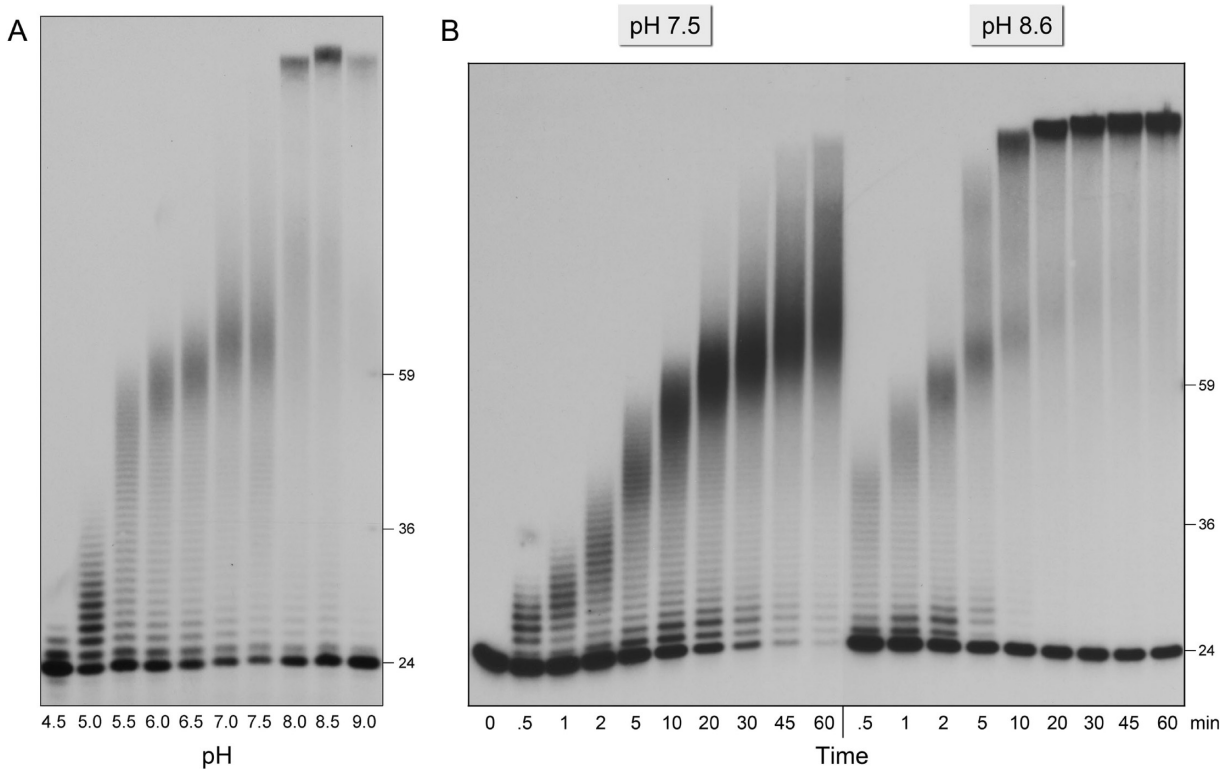

Figure 9. pH and rate profiles of the ΔS1 DNA polymerase activity. (A) Reaction mixtures (10 μL) containing 20 mM Tris buffer (either Tris-acetate pH 4.5−7.0 or Tris-HCl pH 7.5−9.0), 10 mM $MnCl_2$, 2 mM dADP, 0.1 μM (1 pmol) 5′ ^{32}P-labeled 24-mer DNA substrate, and 2 μM (20 pmol) ΔS1 PNPase were incubated for 30 min at 37 °C. (B) Reaction mixtures (90 μL) containing 20 mM Tris-HCl (pH 7.5 or pH 8.6), 5 mM $MnCl_2$, 2 mM dADP, 0.1 μM 5′ ^{32}P-labeled 24-mer DNA substrate, and 2 μM ΔS1 PNPase were incubated at 37 °C. Aliquots (10 μL) were withdrawn at the times specified and quenched immediately with formamide/EDTA. The reaction products were resolved by PAGE and visualized by autoradiography.

was 6-fold less effective (Figure 8D). Taking into account the added metal-independent RNA binding by the full-length PNPase (a property not shared with the deletion variants), the effects of the domain deletions on RNA binding in Mg^{2+} are in accord with their effects on Mg^{2+}-dependent RNA phosphorylase and RNA polymerase activities.

The salient findings in Figure 8E were that subtraction of the S1 domain resulted in a substantial gain-of-function in Mn^{2+}-dependent DNA binding, whereby ΔS1 bound DNA 5-fold better than full-length PNPase. We presume that the enhanced DNA binding by ΔS1 is pertinent to the increased Mn^{2+}-dependent DNA polymerase activity of ΔS1 versus full-length PNPase (Figure 6). By contrast, ΔS1+ΔKH protein was 45-fold less effective in DNA binding in the presence of Mn^{2+} than ΔS1 (Figure 8E), a disparity much greater than the 2-fold differential in Mn^{2+}•dADP-dependent DNA primer extension between ΔS1 and ΔS1+ΔKH (Figure 4B). In the presence of Mg^{2+}, only ΔS1 bound effectively to DNA (Figure 8F).

Characterization of the ΔS1 DNA Polymerase Activity. Primed DNA synthesis by the ΔS1 PNPase was dependent on an added divalent cation (Figure S2A). The metal cofactor requirement was satisfied best by Mn^{2+} (Figure S2A). The efficiency of primer utilization and the length of the poly(dA) tail increased as the Mn^{2+} concentration was raised from 0.625 to 10 mM (Figure S3). A series of divalent cations were tested at 5 mM concentration for their ability of support primed DNA synthesis. Co^{2+} was the second best effector after Mn^{2+}, and it yielded a bimodal distribution of products comprising primers extended by 1−3 nucleotides plus a ladder of longer chains extended by up to 30 nucleotides (Figure S2A). Mg^{2+} was less effective, with respect to primer utilization and the length of the extension tracts (1−10 nucleotides). Ca^{2+} and Ni^{2+} were feeble cofactors. Cu^{2+}, Cd^{2+}, and Zn^{2+} were inactive (Figure S2A). Further insights to metal specificity were gleaned from a mixing experiment in which DNA polymerase reactions containing 5 mM Mn^{2+} were supplemented with 5 mM of a second divalent cation (Figure S2B). Whereas the product distribution in a control reaction containing 10 mM Mn^{2+} was slightly longer than that in 5 mM Mn^{2+} (Figures S2B and S3), the addition of 5 mM Mg^{2+} or 5 mM Ca^{2+} on top of 5 mM Mn^{2+} resulted in the same product profile seen with 5 mM Mn^{2+} alone (Figure S2B). These results suggest that neither Mg^{2+} nor Ca^{2+} competed effectively with Mn^{2+} as a cofactor for DNA synthesis. By contrast, the mixture of Mn^{2+} and Co^{2+} resulted in a product distribution that was a hybrid of the distributions of each metal individually (Figure S2), consistent with either metal being able to satisfy the cofactor requirement. Of the remaining metals that were inactive *per se*, Cu^{2+}, Cd^{2+}, and Zn^{2+} abolished DNA polymerase activity when added to reaction containing an equal concentration of Mn^{2+} (Figure S2B). This result suggests that Cu^{2+}, Cd^{2+}, and Zn^{2+} outcompeted Mn^{2+} for binding to either the enzyme, the dADP substrate, or the DNA primer strand and, when so engaged, completely inhibited DNA synthesis. Ni^{2+} was partially inhibitory (Figure S2B).

The effects of varying dADP concentration are shown in Figure S3. Under the standard reaction conditions (pH 7.5, 5 mM Mn^{2+}), the efficiency of primer utilization by the ΔS1

dx.doi.org/10.1021/bi400281w | *Biochemistry* 2013, 52, 2967−2981

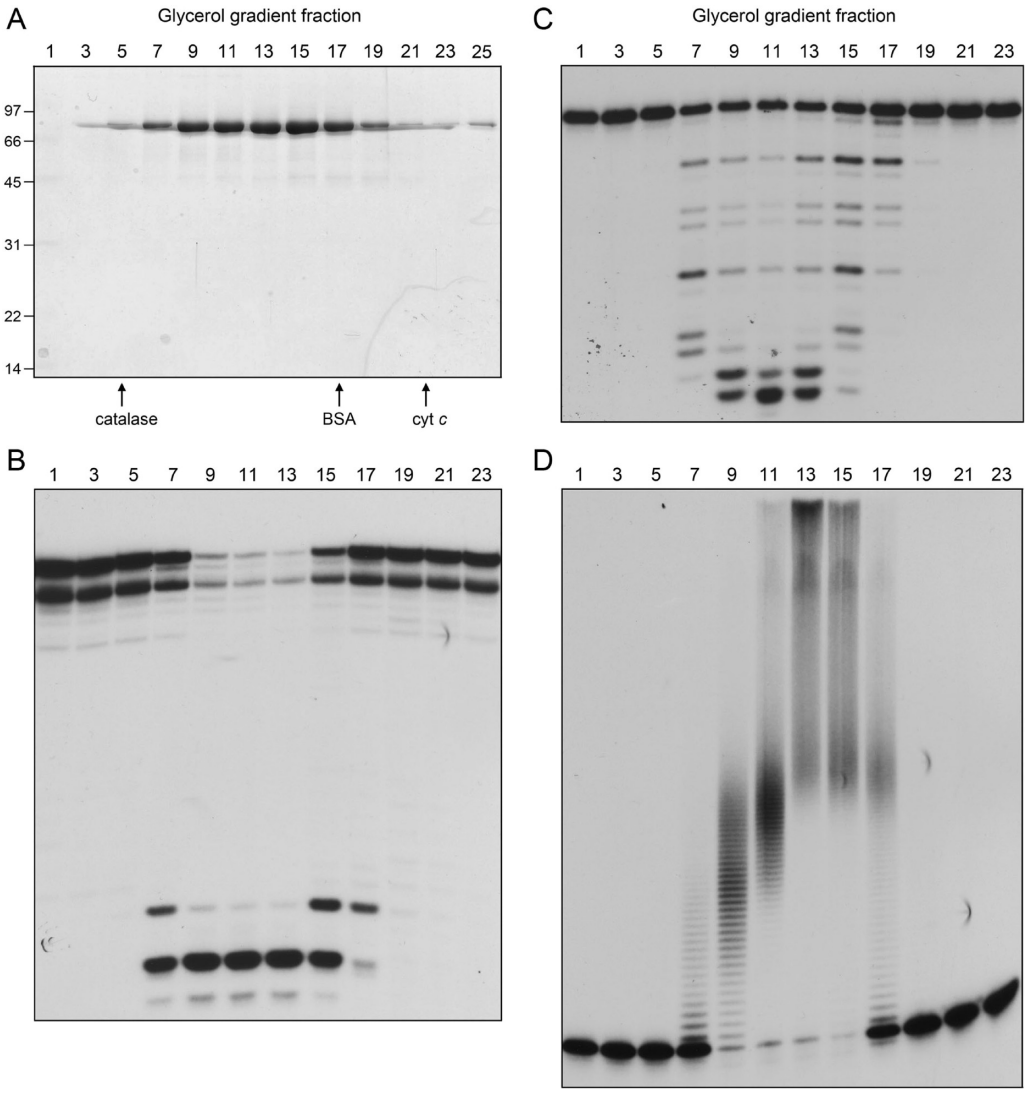

Figure 10. Glycerol gradient sedimentation of ΔS1 PNPase. Δ*S*1 PNPase (660 μg in 74 μL) was applied to a 15−30% glycerol gradient containing 50 mM Tris-HCl (pH 8.0), 200 mM NaCl, 1 mM EDTA. A mixture of catalase (50 μg), BSA (50 μg), and cytochrome *c* (100 μg) was applied to a second glycerol gradient prepared in parallel. The gradients were centrifuged at 50 000 rpm for 16.5 h at 4 °C in a Beckman SW55Ti rotor. Fractions were collected from the bottoms of the tubes. (A) Aliquots (20 μL) of odd-numbered Δ*S*1 PNPase glycerol gradient fractions were analyzed by SDS-PAGE. The Coomassie blue-stained gel is shown. The positions and sizes (in kDa) of molecular-weight markers are indicated on the *left*. The sedimentation peaks of catalase (native size 256 KDa), BSA (native size 66 KDa), and cytochrome *c* (native size 12.3 kDa) that were analyzed in a parallel gradient are indicated by vertical arrows at *bottom*. (B) RNA phosphorylase reaction mixtures (10 μL) containing 20 mM Tris-HCl (pH 7.5), 5 mM $MgCl_2$, 0.5 mM $(NH_4)_2PO_4$, 0.1 μM 5′ ^{32}P-labeled 24-mer RNA substrate, and 2 μL of the indicated glycerol gradient fraction were incubated for 1 h at 37 °C. (C) DNA phosphorylase reaction mixtures (10 μL) containing 20 mM Tris-HCl (pH 7.5), 5 mM $MnCl_2$, 30 μM $(NH_4)_2PO_4$, 0.1 μM 5′ ^{32}P-labeled 24-mer DNA substrate, and 2 μL of the indicated glycerol gradient fraction were incubated for 1 h at 37 °C. (D) DNA polymerase reaction mixtures (10 μL) containing 20 mM Tris-HCl (pH 7.5), 5 mM $MnCl_2$, 2 mM dADP, 0.1 μM 5′ ^{32}P-labeled 24-mer DNA primer, and 2 μL of the indicated glycerol gradient fraction were incubated for 1 h at 37 °C. The reaction products in panels B−D were analyzed by PAGE and visualized by autoradiography.

enzyme and the extension tract length were similar from 0.125 to 2 mM dADP. The extension tract length was diminished at 5 mM dADP and was reduced further at 10 mM dADP (Figure S3). The correlation of the inhibition of DNA primer extension with dADP concentrations equal to or in excess of the input Mn^{2+} suggests that the DNA polymerase requires free Mn^{2+}, i.e., a total Mn^{2+} concentration in excess of the Mn^{2+}•dADP substrate. When tested at 0.2 mM concentration, ADP did not serve as an effective substrate for Mn^{2+}-dependent extension of the DNA primer, i.e., the products made in the presence of ADP were barely longer than those made without added nucleotide (Figure S4). dATP and ATP were also ineffective, as expected (Figure S4).

The Δ*S*1 enzyme was adept at adding poly(dA) tails to ^{32}P-labeled ssDNA primers of varying length (12-mer, 18-mer, 24-mer, or 36-mer) and nucleobase sequence (Figure S5). These ssDNAs also served as primers for the Δ*S*1+ΔKH DNA polymerase, which in each case synthesized shorter poly(dA) tracts than did Δ*S*1 (Figure S5).

pH Effects on Δ*S*1 DNA Polymerase Activity. The pH profile of the DNA polymerase activity is shown in Figure 9A, and revealed distinctive pH effects on the percent of the 24-mer primers extended (maximal at pH 7.0 to 7.5) versus the length

dx.doi.org/10.1021/bi400281w | *Biochemistry* 2013, 52, 2967−2981

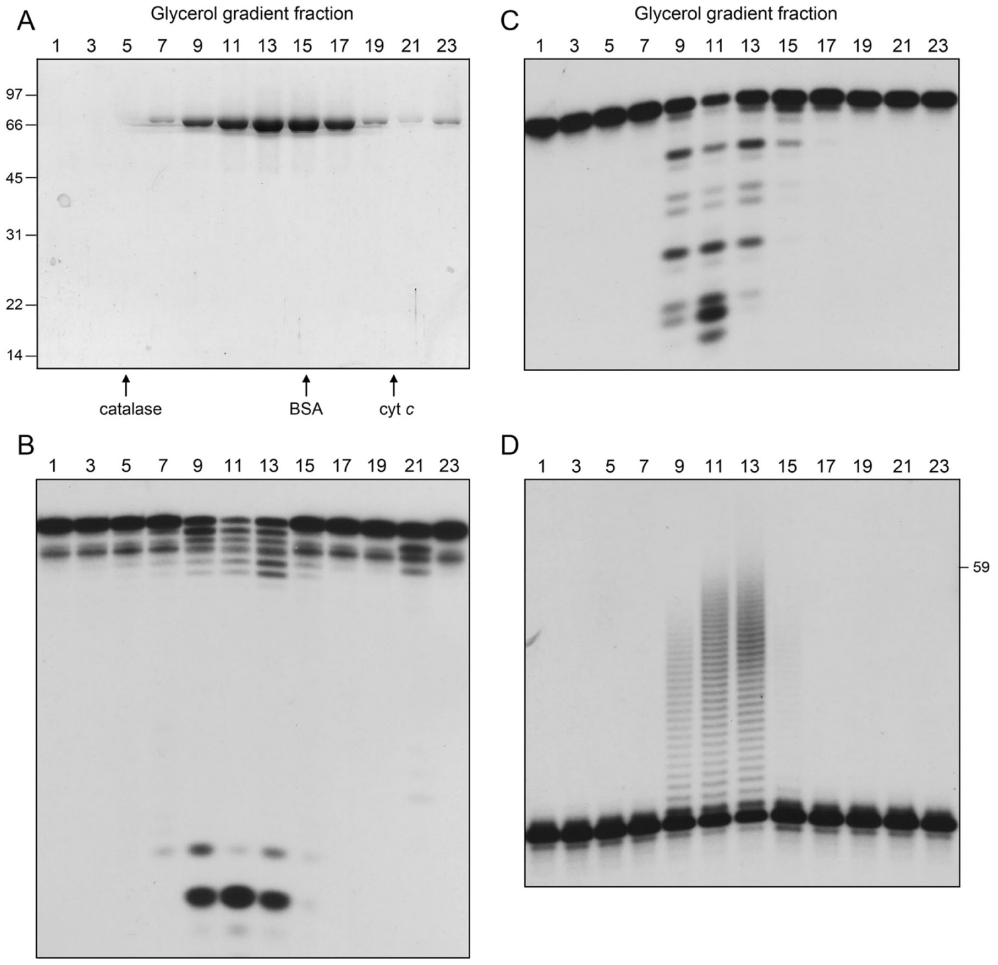

Figure 11. Glycerol gradient sedimentation of ΔS1+ΔKH PNPase. Δ*S*1+ΔKH PNPase (720 μg in 60 μL) was sedimented as described in Figure 10. (A) Aliquots (20 μL) of odd-numbered Δ*S*1+ΔKH PNPase gradient fractions were analyzed by SDS-PAGE. The Coomassie blue-stained gel is shown. The positions and sizes (in kDa) of molecular-weight markers are indicated on the *left*. The sedimentation peaks of catalase, BSA, and cytochrome *c* that were analyzed in a parallel gradient are indicated by vertical arrows at *bottom*. (B–D) RNA phosphorylase (panel B), DNA phosphorylase (panel C), and DNA polymerase (panel D) activities were assayed as described in Figure 10. The reaction products were analyzed by PAGE and visualized by autoradiography.

of the poly(dA) extension tracts synthesized during the 30 min reaction. The Δ*S*1 enzyme generated a cluster of 50–80 nucleotide DNAs at neutral pH. The product sizes decreased gradually as the pH was lowered to 6.5, 6.0, and 5.5, and then declined acutely at pH 5.0 (Figure 9A). Residual activity at pH 4.5 was feeble, with only a minor fraction of the primers being extended and then by only one or two dAMP additions (Figure 9A). By contrast, the product size distribution increased sharply as the pH was raised to 8.0, 8.5, and 9.0, even as the percent primer utilization at alkaline pH declined compared to that at pH 7.0 to 7.5 (Figure 9A).

To better understand this alkaline pH-dependent shift in the polymerase reaction outcomes, we analyzed the kinetics of dAMP addition at pH 7.5 and pH 8.6 (Figure 9B). At pH 7.5, the sizes of the extended primers increased steadily from 0.5 to 10 min. An initial rate of dAMP addition of 10 min^{-1} was deduced from the sizes of the strands at the "leading edge" of the product clusters observed at 0.5 and 1 min (Figure 9B). The rate of subsequent additions declined steadily thereafter, as gauged by the ever smaller marginal size increases between 1 and 2 min, 2 and 5 min, and 5 and 10 min. Product sizes apparently plateaued by 20–30 min in the 50–80 nucleotide range. Note that the fraction of 24-mer primers extended increased steadily for the first 20 min, suggesting that the Δ*S*1 DNA polymerase might experience a kinetic impediment to elongation after a certain number of additions at pH 7.5 and then dissociate to engage a new primer strand. Little further elongation occurred between 30 and 60 min of incubation, a time when essentially all of the input primers had been extended by the Δ*S*1 polymerase (Figure 9B).

The kinetic profile was quite different at pH 8.6. Here the initial rate of dAMP addition estimated from the leading edge of the extended products was 40 min^{-1} (i.e., 4-fold faster than the rate at pH 7.5). The strands initially engaged by the Δ*S*1 enzyme at pH 8.6 were progressively elongated at 1, 2, and 5 min, attaining nearly the same clustered size distribution at 5 min as was seen in a 20 min reaction at pH 7.5. However, the polymerase did not experience a durable kinetic block at pH 8.6, but rather proceeded to elaborate very long poly(dA) tails by 10 and 20 min, which increased in length at 30 and 45 min (albeit not well resolved with respect to size by the PAGE system used). This kinetic pattern is consistent with the Δ*S*1 PNPase displaying enhanced processivity as a DNA polymerase at alkaline versus neutral pH.

Effects of Domain Deletions on PNPase Quaternary Structure. We analyzed the Δ*S*1 PNPase by zonal velocity

dx.doi.org/10.1021/bi400281w | *Biochemistry* 2013, 52, 2967–2981

sedimentation through a 15−30% glycerol gradient. The 73 kDa ΔS1 polypeptide sedimented diffusely in fractions 7−19 and was most abundant in fraction 15 (Figure 10A). Comparison to the peak positions of marker proteins cytochrome *c*, BSA, and catalase sedimented in a parallel gradient (denoted by arrows in Figure 10A) indicated a native size ranging from a ΔS1 monomer to a ΔS1 homotrimer. The peak RNA phosphorylase (Figure 10B) and DNA phosphorylase (Figure 10C) activity was in fractions 9−13, with less activity in flanking fractions 7 and 15, even less in fraction 17, and virtually no activity in fraction 19. The peak DNA polymerase activity (gauged by the extent of primer utilization) was in fractions 9−15 (Figure 10D). This sedimentation profile suggested that subtraction of the S1 domain destabilized the PNPase homotrimer during velocity sedimentation.

This theme was underscored by sedimentation analysis of the ΔS1+ΔKH PNPase (Figure 11). The 66 kDa ΔS1+ΔKH polypeptide sedimented diffusely in fractions 9−17 (Figure 11A). The peaks of ΔS1+ΔKH RNA phosphorylase (Figure 11B), DNA phosphorylase (Figure 11C), and DNA polymerase (Figure 11D) activity were in fractions 9−13, at the leading ("heavy") edge of the protein sedimentation profile, and there was virtually no activity associated with the "light" protein in fractions 15−17. We conclude that the ΔS1+ΔKH quaternary structure is metastable and that the monomeric form of ΔS1+ΔKH (which would peak in fraction 15, as did the 66 kDa BSA marker) is catalytically inactive. Our results for mycobacterial PNPase resonate with an earlier report that the analogous ΔS1+ΔKH truncation of *E. coli* PNPase destabilized its homotrimeric quaternary structure.[3]

Requirements for ΔS1+ΔKH DNA Phosphorylase Activity. The ΔS1+ΔKH PNPase, which was more active as a DNA trimming enzyme than either the full-length or ΔS1 PNPases (Figure S1) was used for further characterization of the DNA phosphorylase reaction. DNA 3′ resection depended on both Mn^{2+} and PO_4; Mg^{2+} was ineffective as the metal cofactor (Figure S6A). Mn^{2+}-dependent DNA phosphorylase activity was optimal at 30−60 μM phosphate and was inhibited at ≥250 mM phosphate (not shown), similar to the low-phosphate optimum and high-phosphate interference seen for the Mn^{2+}-dependent RNA phosphorylase activity of full-length PNPase. (A lower phosphate concentration optimum for Mn^{2+}-dependent phosphorylase activity than for Mg^{2+}-dependent phosphorylase was also reported by the Alonso lab[12,13] in their studies of *Bacillus* PNPase.) The pH profile of the DNA phosphorylase activity was notable for a narrow optimum at pH 7.0−7.5, with little or no 3′ end resection seen at pH ≥8.0 (Figure S6B). The pH profile of the DNA phosphorylase contrasts with that of the DNA polymerase, which is vigorous at pH 8.0 to 8.5. It is conceivable that the synthesis of longer poly(dA) tails by the ΔS1 enzyme at alkaline pH (Figure 9) reflects, in part, the lack of an opposing phosphorylase reaction when phosphate accumulates as a product of DNA synthesis.

DISCUSSION

Our studies of the DNA polymerase and DNA phosphorylase reactions of mycobacterial PNPase contribute to an emerging picture of PNPase as a catalyst of DNA transactions[12,13] in addition to its synthetic and degradative functions in RNA metabolism. The salient findings here are that subtraction of the C-terminal S1 and KH modules elicits unexpected opposite effects on the RNA-modifying and DNA-modifying activities of mycobacterial PNPase.

The DNA polymerase and phosphorylase activities of mycobacterial PNPase prefer manganese as the metal cofactor, unlike the RNA polymerase and phosphorylase activities for which magnesium suffices. Although changes in the substrate preferences of nucleic acid enzymes in response to varying the divalent cation are often dismissed as *in vitro* quirks, our experience with enzymes that mediate bacterial NHEJ and bacterial RNA repair has taught us that the ligase, polymerase, 3′-phosphoesterase, and methyltransferase components of these repair pathways require manganese for catalysis and are either inactive or poorly active with magnesium.[26−34] Studies of the radio-resistant bacterium *Deinococcus* have revealed that manganese exerts profound effects on its sensitivity to radiation and oxidative stress *in vivo*.[35,36] The observed ablation of both the Mn^{2+} and Mg^{2+} dependent activities of mycobacterial PNPase by the D526A mutation argues that they bind to the same site on the enzyme, corresponding to the site defined by the crystal structure of an *E. coli* PNPase•Mn^{2+} complex.[4] Definitive insights to the correlated metal and polynucleotide specificities of PNPase will necessarily hinge on obtaining crystal structures of PNPase enzymes in complexes with metals and RNA or DNA strands (of otherwise identical length and nucleobase sequence) in the enzyme active site.

Our analysis of the effects of S1 and KH domain deletions on the RNA transactions of mycobacterial PNPase are in keeping with analogous findings for other bacterial PNPases. To wit, that subtracting the S1 domain diminishes RNA phosphorylase and polymerase activity and that simultaneous deletion of the S1 and KH domains further cripples the enzyme with respect to RNA substrates.[3,8] The consensus hypothesis that the S1 and KH domains bind RNA and direct the polynucleotide 3′ end into the central channel of the PNPase homotrimer was validated by the recent crystal structure of *Caulobacter* PNPase, which highlights atomic contacts of the KH domain to a 5-nucleotide RNA segment situated immediately above the channel entrance.[6] The KH−RNA interface entails van der Waals and hydrophilic interactions of side chain and main chain atoms of all three KH modules with RNA sugars, nucleobases, and phosphates. The aliphatic residues in the *Caulobacter* KH domain that make van der Waals contacts with the RNA are conserved in the *M. smegmatis* PNPase KH domain (as Ile604, Ile608, Ile615, and Ile626). The RNA interactions of the S1 domain are uncharted.

Our unexpected findings that S1 and KH domain deletions enhance the DNA polymerase and phosphorylase activity of mycobacterial PNPase add a new dimension to our understanding of PNPase specificity, whereby the C-terminal modules serve a dual purpose: (i) to help capture an RNA polynucleotide substrate for processive 3′ end-processing, and (ii) to act as a specificity filter that selects against a DNA polynucleotide substrate. The simplest interpretation is that subtraction of the S1 and KH modules leads to enhanced DNA end-processing by eliminating the inherent RNA advantage provided by one or both of those domains. Our experiments using a gel-shift assay to score nucleic acid binding to mycobacterial PNPase point to the S1 domain as the RNA selectivity filter, by virtue of its ability to confer RNA-specific binding in the absence of a divalent cation. When the S1 domain is deleted, the ΔS1 PNPase binds to either RNA or DNA in a distinct mode that requires a divalent cation.

It is possible that additional effects of the C-terminal domain deletions on the structure of the central channel might also play a role in the gain of DNA reactivity. For example, when Shi et

al.[3] determined and compared the crystal structures of full-length *E. coli* PNPase and truncated ΔS1+ΔKH PNPase, they noted that the central channel was wider in ΔS1+ΔKH. Perhaps the wider channel in the ΔS1+ΔKH PNPase can better accommodate a DNA polynucleotide than does full-length PNPase.

To date, mycobacterial PNPase has received little attention. The lone published study of a mycobacterial PNPase enzyme (isolated from *M. tuberculosis*) dates from 1964.[37] The genetics of mycobacterial PNPase are untouched. The *Rv2783c* gene encoding *M. tuberculosis* PNPase is located within a cluster of co-oriented open reading frames in the order: *rpsO* (encoding ribosomal protein S15), *lppU* (a liporotein), *Rv2783c* (PNPase), *pepR* (a zinc protease), and *Rv2781c* (a putative oxidoreductase). The upstream *lppU* gene and the downstream *pepR* and *Rv2781c* genes are deemed inessential for *M. tuberculosis* growth, as defined by the recovery of viable bacteria with transposon insertions within these respective open reading frames.[38] By contrast, no transposon insertion within the PNPase gene was recovered,[38] raising the prospect that PNPase might be essential for growth of *M. tuberculosis* under laboratory conditions. In that case, PNPase would merit consideration as (i) a target for inhibitor discovery and (ii) for a genetic dissection of the impact of the PNPase mutations characterized herein on mycobacterial growth and physiology.

■ ASSOCIATED CONTENT

Supporting Information

Supplemental Figures S1−S6. This material is available free of charge via the Internet at http://pubs.acs.org

■ AUTHOR INFORMATION

Corresponding Author

*Phone: 212-639-7145; e-mail: s-shuman@ski.mskcc.org.

Notes

The authors declare no competing financial interest.

■ ACKNOWLEDGMENTS

This research was supported by NIH Grant AI64693. S.S. is an American Cancer Society Research Professor.

■ REFERENCES

(1) Mohanty, B. K., and Kushner, S. R. (2000) Polynucleotide phosphorylase functions both as a 3′-to-5′ exonuclease and a poly(A) polymerase in *Escherichia coli*. *Proc. Natl. Acad. Sci. U. S. A. 97*, 11966−11971.

(2) Symmons, M. F., Jones, G. H., and Luisi, B. F. (2000) A duplicated fold is the structural basis for polynucleotide phosphorylase catalytic activity, processivity, and regulation. *Structure 8*, 1215−1226.

(3) Shi, Z., Yang, W. Z., Lin-Chao, S., Chak, K. F., and Yuan, H. S. (2008) Crystal structure of *Escherichia coli* PNPase: central channel residues are involved in processive RNA degradation. *RNA 14*, 2361−2371.

(4) Nurmohamed, S., Vaidialingam, B., Callaghan, A. J., and Luisi, B. F. (2009) Crystal structure of *Escherichia coli* polynucleotide phosphorylase core bound to RNase E, RNA and manganese: implications for catalytic mechanism and RNA degradosome assembly. *J. Mol. Biol. 389*, 17−33.

(5) Lin, C. H., Wang, y.T., Yang, W. Z., Hsiao, Y. Y., and Yuan, H. S. (2012) Crystal structure of human polynucleotide phosphorylase: insights into its domain function in RNA binding and degradation. *Nucleic Acids Res. 40*, 4146−4157.

(6) Hardwick, S. W., Gubbey, T., Hug, I., Jenal, U., and Luisi, B. F. (2012) Crystal structure of *Caulobacter crescentus* polynucleotide phosphorylase reveals a mechanism of RNA substrate channeling and RNA degradosome assembly. *Open Biol. 2*, 120028.

(7) Jarrige, A. C., Brechemier-Baey, D., Mathy, N., Duche, O., and Portier, C. (2002) Mutational analysis of polynucleotide phosphorylase from *Escherichia coli*. *J. Mol. Biol. 321*, 397−409.

(8) Stickney, L. M., Hankins, J. S., Miao, X., and Mackie, G. A. (2005) Function of the conserved S1 and KH domains in polynucleotide phosphorylase. *J. Bacteriol. 187*, 7214−7221.

(9) Chou, J. Y., and Singer, M. F. (1971) Deoxyadenosine diphosphate as a substrate and inhibitor of polynucleotide phosphorylase of *Micrococcus luteus*. *J. Biol. Chem. 246*, 7486−7496.

(10) Kaufmann, G., and Littauer, U. Z. (1969) Deoxyadenosine diphosphate as substrate for polynucleotide phosphorylase from *Escherichia coli*. *FEBS Lett. 4*, 79−83.

(11) Beljanski, M. (1996) *De novo* synthesis of DNA-like molecules by polynucleotide phosphorylase *in vitro*. *J. Mol. Evol. 42*, 493−499.

(12) Cardenas, P. P., Carrasco, B., Sanchez, H., Deikus, G., Bechhofer, D. H., and Alonso, J. C. (2009) *Bacillus subtilis* polynucleotide phosphorylase 3′-to-5′ DNase activity is involved in DNA repair. *Nucleic Acids Res. 37*, 4157−4169.

(13) Cardenas, P. P., Carzaniga, T., Zangrossi, S., Briani, F., Garcia-Tirado, E., Deho, G., and Alonso, J. C. (2011) Polynucleotide phosphorylase exonuclease and polymerase activities on single-stranded DNA ends are modulated by RecN, SsbA and RecA proteins. *Nucleic Acids Res. 39*, 9250−9261.

(14) Rath, D., Mangoli, S. H., Pagedar, A. R., and Jawali, N. (2012) Involvement of *pnp* in survival of UV radiation in *Escherichia coli* K-12. *Microbiology 158*, 1196−1205.

(15) Becket, E., Tse, L., Yung, M., Cosico, A., and Miller, J. H. (2012) Polynucleotide phosphorylase plays an important role in the generation of spontaneous mutations in *Escherichia coli*. *J. Bacteriol. 194*, 5613−5620.

(16) Gupta, R., Barkan, D., Redelman-Sidi, G., Shuman, S., and Glickman, M. S. (2011) Mycobacteria exploit three genetically distinct DNA double-strand break repair pathways. *Mol. Microbiol. 79*, 316−330.

(17) Gupta, R., Ryzhikov, M., Koroloeva, O., Unciuleac, M., Shuman, S., Korolev, S., and Glickman, M. S. (2012) A dual role for mycobacterial RecO in RecA-dependent homologous recombination and RecA-independent single-strand annealing. *Nucleic Acids Res. 41*, 2284−2295.

(18) Ayora, S., Carrasco, B., Cárdenas, P. P., César, C. E., Cañas, C., Yadav, T., Marchisone, C., and Alonso, J. C. (2011) Double-strand break repair in bacteria: a view from *Bacillus subtilis*. *FEMS Microbiol. Rev. 35*, 1055−1081.

(19) Shuman, S., and Glickman, M. S. (2007) Bacterial DNA repair by non-homologous end joining. *Nat. Rev. Microbiol. 5*, 852−861.

(20) Gong, C., Bongiorno, P., Martins, A., Stephanou, N. C., Zhu, H., Shuman, S., and Glickman, M. S. (2005) Mechanism of non-homologous end joining in mycobacteria: a low-fidelity repair system driven by Ku, ligase D and ligase C. *Nat. Struct. Mol. Biol. 12*, 304−312.

(21) Aniukwu, J., Glickman, M. S., and Shuman, S. (2008) The pathways and outcomes of mycobacterial NHEJ depend on the structure of the broken DNA ends. *Genes Dev. 22*, 512−527.

(22) Akey, D., Martins, A., Aniukwu, J., Glickman, M. S., Shuman, S., and Berger, J. M. (2006) Crystal structure and nonhomologous end joining function of the ligase domain of *Mycobacterium* DNA ligase D. *J. Biol. Chem. 281*, 13412−13423.

(23) Zhu, H., Nandakumar, J., Aniukwu, J., Wang, L. K., Glickman, M. S., Lima, C. D., and Shuman, S. (2006) Atomic structure and nonhomologous end-joining function of the polymerase component of bacterial DNA ligase D. *Proc. Natl. Acad. Sci. U. S. A. 103*, 1711−1716.

(24) Pitcher, R. S., Brissett, N. C., Picher, A. J., Andrade, P., Juarez, R., Thompson, D., Fox, G. C., Blanco, L., and Doherty, A. J. (2007) Structure and function of a mycobacterial NHEJ DNA repair polymerase. *J. Mol. Biol. 366*, 391−405.

(25) Nair, P. A., Smith, P., and Shuman, S. (2010) Structure of bacterial LigD 3′-phosphoesterase unveils a DNA repair superfamily. *Proc. Natl. Acad. Sci. U. S. A. 107*, 12822−12827.

(26) Zhu, H., and Shuman, S. (2005) A primer-dependent polymerase function of *Pseudomonas aeruginosa* ATP-dependent DNA ligase (LigD). *J. Biol. Chem. 280*, 418−427.
(27) Zhu, H., and Shuman, S. (2005) Novel 3′-ribonuclease and 3′-phosphatase activities of the bacterial non-homologous end-joining protein, DNA ligase D. *J. Biol. Chem. 280*, 25973−25981.
(28) Zhu, H., and Shuman, S. (2007) Characterization of *Agrobacterium tumefaciens* DNA ligases C and D. *Nucleic Acids Res. 35*, 3631−3645.
(29) Das, U., Smith, P., and Shuman, S. (2012) Structural insights to the metal specificity of an archaeal member of the LigD 3′-phosphoesterase DNA repair enzyme family. *Nucleic Acids Res. 40*, 828−836.
(30) Martins, A., and Shuman, S. (2004) An RNA ligase from *Deinococcus radiodurans*. *J. Biol. Chem. 279*, 50654−50661.
(31) Martins, A., and Shuman, S. (2005) An end-healing enzyme from *Clostridium thermocellum* with 5′ kinase, 2′,3′ phosphatase, and adenylyltransferase activities. *RNA 11*, 1271−1280.
(32) Keppetipola, N., and Shuman, S. (2006) Distinct enzymic functional groups are required for the phosphomonoesterase and phosphodiesterase activities of *Clostridium thermocellum* polynucleotide kinase/phosphatase. *J. Biol. Chem. 281*, 19251−19259.
(33) Jain, R., and Shuman, S. (2010) Bacterial Hen1 is a 3′ terminal RNA ribose 2′O-methyltransferase component of a bacterial RNA repair cassette. *RNA 16*, 316−323.
(34) Jain, R., and Shuman, S. (2011) Active site mapping and substrate specificity of bacterial Hen1, a manganese-dependent 3′ terminal RNA ribose 2′O-methyltransferase. *RNA 17*, 429−438.
(35) Daly, M. J. (2009) A new perspective on radiation resistance based on *Deinococcus radiodurans*. *Nat. Rev. Microbiol. 7*, 237−245.
(36) Slade, D., and Radman, M. (2011) Oxidative stress resistance in *Deinococcus radiodurans*. *Microbiol. Mol. Biol. Rev. 75*, 133−191.
(37) Malathi, V. G., Sirsi, M., Ramakrishnan, T., and Maller, R. K. (1964) Polynucleotide phosphorylase of Mycobacterium tuberculosis H37Rv. *Indian J. Biochem. 1*, 71−76.
(38) Sassetti, C. M., Boyd, D. H., and Rubin, E. J. (2003) Genes required for mycobacterial growth defined by high density mutagenesis. *Mol. Microbiol. 48*, 77−84.